

# CHEMISTRY

## A European Journal

A Journal of



### Accepted Article

**Title:** Tuning the pKa of Fluorescent Rhodamine pH Probes via Substituent Effects

**Authors:** Sarah G. Stratton, Grace H. Taumoefolau, Grace E. Purnell, Mona Rasooly, William L. Czaplyski, and Elizabeth J. Harbron

This manuscript has been accepted after peer review and appears as an Accepted Article online prior to editing, proofing, and formal publication of the final Version of Record (VoR). This work is currently citable by using the Digital Object Identifier (DOI) given below. The VoR will be published online in Early View as soon as possible and may be different to this Accepted Article as a result of editing. Readers should obtain the VoR from the journal website shown below when it is published to ensure accuracy of information. The authors are responsible for the content of this Accepted Article.

**To be cited as:** *Chem. Eur. J.* 10.1002/chem.201703176

**Link to VoR:** <http://dx.doi.org/10.1002/chem.201703176>

Supported by  
**ACES**

WILEY-VCH

## Tuning the $pK_a$ of Fluorescent Rhodamine pH Probes via Substituent Effects

Sarah G. Stratton,<sup>[a]</sup> Grace H. Taumoefolau,<sup>[a]</sup> Grace E. Purnell,<sup>[a]</sup> Mona Rasooly,<sup>[a]</sup>  
William L. Czaplowski,<sup>[a]</sup> and Elizabeth J. Harbron<sup>\*[a]</sup>

**Abstract:** Rhodamine spirolactams (RSLs) have recently emerged as popular fluorescent pH probes due to their fluorescence turn-on capability and ease of functionalization at the spirolactam nitrogen. Design of RSLs is often driven by biological targeting or compatibility concerns rather than the pH sensitivity of the probe, and the relationship between RSL structure and  $pK_a$  is not well-understood. Here we present a series of 19 aniline-derived RSLs designed to elucidate the relationship between  $pK_a$  values and the properties of substituents attached to the spirolactam nitrogen. RSLs derived from di-*ortho*-substituted anilines exhibit  $pK_a$  tunability across the moderately acidic region (ca. pH 4 – 6). Evaluation of  $pK_a$  data using the Fujita-Nishioka model for *ortho* substituent effects reveals that both steric and electronic substituent properties influence RSL pH responsiveness, with  $pK_a$  values increasing as substituent size and electron withdrawing character increase. These trends are attributed to changes in the RSL structure induced by large substituents and to electronic influences on the protonated spirocyclic reaction intermediate. To demonstrate the practical applicability of these probes in completely aqueous environments, we present RSL-doped conjugated polymer nanoparticles, which exhibit a ratiometric fluorescence response to changing pH levels.

[a] S.G. Stratton, G.H. Taumoefolau, G.E. Purnell, M. Rasooly, W.L. Czaplowski, Prof. E.J. Harbron  
Department of Chemistry  
The College of William and Mary  
Williamsburg, VA 23187-8795 (USA)  
E-mail: ejharb@wm.edu

## Introduction

Accurate measurement of pH is crucial to understanding the many chemical and biological processes that are influenced by proton concentration. Microelectrodes, magnetic resonance techniques, and optical spectroscopy are among the methods routinely used to measure pH.<sup>[1]</sup> From this group, fluorescence spectroscopy has emerged as the method of choice for samples with spatial variation in pH.<sup>[2]</sup> Cells exemplify this type of sample: the pH required for normal function ranges from alkaline (pH 8.0) in mitochondria to near-neutral in the cytosol to acidic in lysosomes (pH 4.7).<sup>[3]</sup> An exquisite balance of biochemical processes is required to maintain cellular pH levels,<sup>[3]</sup> and deviations from normal pH levels are associated with diseases such as cancer.<sup>[4]</sup> Fluorescence can report on cellular pH values nondestructively and with high spatiotemporal resolution and sensitivity.<sup>[2]</sup> Measurement of pH by fluorescence spectroscopy utilizes probes with emission properties that are strongly pH-dependent.<sup>[2, 5]</sup> Based on their  $pK_a$  values, fluorescent pH probes for intracellular measurements are generally divided into those useful in near-neutral (ca. pH 7) and acidic (pH 4.5-6) environments. Although probes that are sensitive to acidic environments are critical for tracking processes within acidic organelles, fewer have been developed compared to those for near-neutral environments.<sup>[6]</sup>

Rhodamine spirolactams (RSLs) show remarkable promise as fluorescent pH probes for acidic environments. As shown in Scheme 1 for a generic rhodamine B derivative, RSLs exhibit a pH-dependent equilibrium between two forms, the colorless and non-fluorescent spirolactam and the colored and fluorescent rhodamine amide. Off-to-on colorimetric and fluorescence switching is observed as the RSLs' environment becomes more acidic, triggering opening of the spirocyclic ring system to reveal the fully conjugated rhodamine dye. The fluorescent form of the RSL possesses all of the desirable photophysical characteristics of its parent rhodamine dye, including excitation and emission in the visible region of the spectrum, high extinction coefficient, high fluorescence quantum yield, and good photostability.<sup>[7]</sup>

Due to these outstanding photophysical properties, RSL-based pH probes have proliferated in the last few years and have been featured in reviews.<sup>[6, 8]</sup> Recent examples include RSLs for the single-wavelength monitoring of pH fluctuations in lysosomes<sup>[9]</sup> and other biological environments,<sup>[10]</sup> an RSL-fluorescein construct for wide range pH monitoring,<sup>[11]</sup> and RSL-containing dyads for ratiometric pH measurements.<sup>[12]</sup> Acid-responsive RSLs have also been incorporated into macromolecular systems for pH sensing,<sup>[13]</sup> tumor imaging,<sup>[14]</sup> and

anticancer drug release.<sup>[15]</sup> The  $pK_a$  values of RSLs vary with the spirolactam R group, with many rhodamine B-derived probes intended for acidic pH monitoring falling in the pH 4-5 range. Selection of the R group tends to be driven by concerns such as organelle targeting rather than the goal of obtaining a specific  $pK_a$  value. While this approach addresses biological compatibility, it does not enable the targeting of specific processes for pH monitoring by RSLs. Towards this end, we seek a systematic understanding of the structure- $pK_a$  relationship for RSLs.

Substituent effects on chemical reactivity can be driven by steric or electronic interactions or a combination of both. Both steric and electronic effects have previously been cited as influences on the pH-responsiveness of RSLs and related compounds. Yuan, et al. found that RSLs with sterically demanding spirolactam R groups had higher  $pK_a$  values than those with smaller substituents.<sup>[16]</sup> In our own work, identical  $pK_a$  values were observed across a series of RSLs derived from *para*-substituted anilines with different substituents.<sup>[17]</sup> However, one derivative prepared with a bulkier 2,4,6-substituted aniline exhibited a much higher  $pK_a$  value, supporting the finding of Yuan. These results provide anecdotal evidence that the pH-responsiveness of RSLs can be tuned by controlling steric bulk near the spirolactam nitrogen. This finding is in contrast to the behavior of rhodamine deoxy-lactams, RSL derivatives in which the spirolactam carbonyl moiety has been removed. The pH-responsiveness of the deoxy-lactams is correlated with the basicity of amine functionality, and both electronic<sup>[18]</sup> and steric<sup>[19]</sup> effects on the basicity have been documented.

We seek to establish a structure-property relationship for the  $pK_a$  values of RSL pH probes for acidic environments. Here we present a series of aniline-derived RSLs in which the substituents near the spirolactam nitrogen are varied in position and steric and electronic properties. Upon establishing the tunability of  $pK_a$  values, we employ simple and multiple linear regression models to explore the origin of their variance. We also demonstrate the practical utility of RSLs for ratiometric pH sensing in a completely aqueous environment by preparing RSL-doped conjugated polymer nanoparticles.

## Results and Discussion

RSL derivatives **1-19** (Table 1) were designed to probe the influence of the spirolactam R group on the spirocyclic ring-opening reaction. To facilitate variation of substituent steric and electronic properties, the R group was derived from substituted anilines and is denoted Ar in

Scheme 2. The rhodamine scaffold of RSL-based pH probes is commonly derived from rhodamine B (RB) or rhodamine 6G (R6G), which differ in the substitution pattern of the xanthene ring system (Scheme 2) and in their fluorescent properties. To address hypotheses generated by our previous work on related derivatives,<sup>[17]</sup> we derived most of our compounds (**1-13**) from RB, which fluoresces yellow-orange. With our long-term interest in fluorescence resonance energy transfer (FRET), RB derivatives are also attractive as acceptor dyes due to their low energy fluorescence.<sup>[20]</sup> Additionally, we prepared a smaller series of compounds based on R6G (**14-19**), which emits green fluorescence with a much higher quantum yield than RB.<sup>[21]</sup> The additional methyl substituents on R6G's xanthene moiety facilitate exploration of the combined effects of steric hindrance in the spiro lactam substituent and the xanthene core. Compounds **1-19** were prepared from the desired aniline and RB or the carboxylic acid form of R6G via the rhodamine acid chloride. Structures of the RSLs were verified by high resolution mass spectrometry and <sup>1</sup>H and <sup>13</sup>C NMR. All compound exhibited the characteristic resonance of the spiro carbon in the <sup>13</sup>C NMR spectrum (67.5 – 70.3 ppm for **1-19**), verifying their spirocyclic structures.

Consistent with other RSL derivatives, compounds **1-19** are all colorless and non-fluorescent in their as-prepared spirocyclic forms, which absorb only in the ultraviolet with peaks ca. 275 and 315 nm. Accordingly, they exhibit no absorbance or fluorescence in the visible region of the spectrum. Addition of acid opens the spiro lactam moiety to reveal the highly colored and fully conjugated rhodamine dye structure (Scheme 1). The increases in visible absorbance and fluorescence intensity upon HCl addition are shown in Figure 1 for representative RB derivative **9**, which has  $\lambda_{\text{max,abs}}$  and  $\lambda_{\text{max,fl}}$  values of 561 and 581 nm, respectively. These values are typical for RB derivatives **1-13**, which all have spectral maxima within 561-563 nm for absorbance and 581-585 nm for fluorescence (Table S1). R6G derivatives have similarly clustered values with ranges 532-533 nm and 551-555 nm for absorbance and fluorescence, respectively. For both RB and R6G derivatives, there is no consistent trend in  $\lambda_{\text{max,abs}}$  and  $\lambda_{\text{max,fl}}$  values with respect to the steric and electronic properties of the aniline substituents.

We divided the RSLs into 4 overlapping series to facilitate comparison of pH-responsiveness among the different derivatives. Series 1, comprised by RB derivatives **1-4** and **10**, was designed to elucidate the aniline substitution pattern required to induce steric effects on

the  $pK_a$ . The  $pK_a$  value for each compound was determined via fluorescence titration with HCl. From fluorescence spectra recorded after each addition of acid, the fluorescence intensity at the  $\lambda_{\text{max,fl}}$  was extracted and plotted as a function of pH to construct a titration curve. The  $pK_a$  is then determined by calculating the pH at which the fluorescence intensity is half of its maximum value. Figure 2 shows representative titration curves for Series 1 compounds, all of which contain 1 or 2 chlorine substituents in different positions relative to the aniline nitrogen, which is part of the spirolactam ring in the closed form of the RSL. Substitution of Cl at the *para* position (**1**), both *meta* positions (**3**), or a single *ortho* position (**10**) gave nearly indistinguishable  $pK_a$  values near 4.3, which is also the value obtained for an unsubstituted control (**5**). In contrast, chlorine substitution of both *ortho* positions (**4**) or both *ortho* positions with a *para*-nitro substituent (**2**) gave significantly shifted titration curves with  $pK_a$  values that are identical within experimental error at ca. 5.4. Series 1 compounds demonstrate that both *ortho* positions of the aniline-derived ring must be substituted to effect a significant shift in the  $pK_a$  from “baseline” values for aniline-derived RSLs, shown here to be ca. 4.3.

To determine the extent to which di-*ortho* substitution can be used to tune the  $pK_a$  of aniline-derived RSLs, we prepared additional di-*ortho*-substituted derivatives based on RB (Series 2, **4-9**) and R6G (Series 3, **14-19**). Substituents were selected from commercially available di-*ortho*-substituted anilines to cover a range of steric and electronic substituent properties. Titration curves for RB Series 2 compounds (Figure 3A) are distributed across the acidic region, demonstrating a clear substituent dependence. The  $pK_a$  values extracted from these curves range from a low of 4.03 (**7** OEt) to a high of 5.72 (**9** iPr), a span of 1.7 pH units (Table 1). R6G Series 3 titration curves (Figure 3B) span a slightly greater range of values than their RB Series 2 counterparts, from a low of 3.81 (**15** H) to a high of 5.87 (**19** iPr), a difference of 2.1 pH units. Unlike the fairly even distribution of  $pK_a$  values observed for Series 2, Series 3  $pK_a$  values are more clustered, with the compounds having the highest  $pK_a$  values (**14**, **18**, **19**) narrowly distributed around an average of 5.60. We expected that R6G Series 3 would yield higher  $pK_a$  values than RB Series 2 due to steric hindrance from the additional methyl group on the xanthene core of R6G. Indeed, identical substituents yielded higher  $pK_a$  values in R6G than RB for four of the six compounds, with the greatest difference between di-*ortho*-methyl-substituted **8** and **18** ( $\Delta pK_a = 0.42$ ). This trend is consistent with the work of Yuan, et al., who observed an even larger  $pK_a$  difference between R6G and RB derivatives in which the

spirolactam nitrogen was functionalized with an adamantyl group.<sup>[16]</sup> The Series 2 and 3 compounds demonstrate that we can use substituent effects to manipulate the  $pK_a$  across the acidic region.

Our ultimate goal is to define a structure-property relationship for the pH-responsiveness of RSLs. Linear free energy relationships (LFERs) can supply a quantitative understanding of how substituent properties influence a reaction or molecular property. To test our initial hypothesis that increasing steric hindrance at the spirolactam nitrogen would increase the  $pK_a$  of RSLs, we examined univariate correlations of our Series 2 and 3  $pK_a$  data with standard steric parameters. The steric parameters<sup>[22]</sup> included in this analysis were  $A$ -values (Winstein-Holness values), Charton's  $\nu$ , Meyer's  $V^a$ , interference values, Sterimol  $B_1$  values, and Taft  $E_S$  values<sup>[23]</sup> as modified by Kutter and Hansch.<sup>[24]</sup> The extent of correlation between the  $pK_a$  values and substituent steric properties varied considerably depending on the steric parameter used. Three parameters – Sterimol  $B_1$ , interference values, and  $E_S$  – yielded correlations for which the  $r^2$  value was greater than 0.6 for both Series 2 and 3 data. The strongest correlation was observed for  $E_S$  (Figure 4), which is correlated with substituents' van der Waals radii.<sup>[24]</sup> The  $E_S$ - $pK_a$  correlation was more significant and had a steeper slope for R6G Series 3 than for RB Series 2, suggesting that steric effects might be more dominant for R6G compounds. However, the significant scatter in Figure 4 indicates that steric properties alone cannot account for the observed range of  $pK_a$  values in Series 2 and 3.

The scatter in the univariate correlations suggests that both electronic and steric substituent properties may influence the  $pK_a$  values. Several LFERs have been developed for the treatment of data for *ortho*-substituted compounds, which may have steric, inductive, and resonance effects that are distinct from those with more distant *meta* and *para* substituents. Building on the work of Taft<sup>[23]</sup> and Charton,<sup>[25]</sup> Fujita and Nishioka developed a 3-parameter LFER for *ortho* effects.<sup>[26]</sup> Their original model divides the effect of *ortho* substituents into contributions from ordinary polar, proximity polar, and steric effects to yield Equation 1, where  $\sigma_o$ ,  $F$ , and  $E_s$  are substituent parameters, and  $\rho$ ,  $f$ , and  $\delta$  are the respective susceptibility constants.<sup>[26]</sup> The ordinary polar effect encompasses both inductive and resonance effects and is

$$\log k_o = \rho\sigma_o + fF + \delta E_s + c \quad (1)$$

given by  $\sigma_o \equiv \sigma_p$ , the standard Hammett constant. The Swain-Lupton field parameter  $F$ <sup>[27]</sup> is used to correct for the greater inductive and field effects of *ortho* over *para* substituents, and the Taft-Kutter-Hansch  $E_s$  values are used as the steric parameter. Alternatively, the Fujita-Nishioka model can be reformulated<sup>[26]</sup> to express electronic effects as a linear combination of field and resonance effects as shown in Equation 2, where  $R$  is the Swain-Lupton-Hansch resonance

$$\log k_o = fF + rR + \delta E_s + c \quad (2)$$

parameter<sup>[27-28]</sup> and  $f$ ,  $r$ , and  $\delta$  are the susceptibility constants for the field, resonance, and steric parameters. Eqs. 1 and 2 have successfully accounted for substituent effects on kinetics, thermodynamics, and chemical shifts.<sup>[26]</sup>

Multiple linear regressions of Series 2 and 3 data were performed according to Eqs. 1 and 2 using literature values for  $\sigma$ ,  $E_s$ ,  $F$ , and  $R$  (Table 2) with the value of each substituent constant doubled to account for the di-*ortho* substitution of these compounds.<sup>[29]</sup> The Fujita-Nishioka models given by Eqs. 1 and 2 yielded significant correlations, explaining 95% and 98% of the variance in  $pK_a$  values for RB and R6G derivatives, respectively. As shown in Eqs. 3A (RB) and 3B (R6G), regression by Eq. 1 curiously yields electronic coefficients with opposite signs. The

$$pK_a = 1.25\sigma_p - 0.44F - 0.48E_s + 4.28 \quad (R^2 = 0.953) \quad (3A)$$

$$pK_a = 1.05\sigma_p - 0.21F - 0.72E_s + 3.82 \quad (R^2 = 0.983) \quad (3B)$$

positive value for  $\rho$  indicates that  $pK_a$  values increase as the electron withdrawing nature of the substituent increases, but the negative value for  $f$  indicates the opposite trend. This result suggests that regression by Eq. 1 may overestimate the influence of inductive and field effects and underestimate the contribution of resonance effects to the  $pK_a$  values. Indeed, regression by Eq. 2 with separate field and resonance parameters yields coefficients with the same sign that paint a more consistent picture, as shown in Eqs. 4A (RB) and 4B (R6G). Regression according to Charton's model, which also uses separate parameters for inductive and resonance effects, gives extremely similar results with high significance (Figure S3), validating the use of Eq. 2 for our system.

$$pK_a = 0.72F + 1.26R - 0.47E_s + 4.28 \quad (R^2 = 0.953) \quad (4A)$$

$$pK_a = 0.78F + 1.06R - 0.72E_s + 3.82 \quad (R^2 = 0.983) \quad (4B)$$

Figure 5 depicts the excellent agreement between experimental and predicted values for regression of Series 2 and 3 by Eq. 2. To evaluate the relative contributions of field, resonance, and steric effects to the  $pK_a$  values, we determined the standardized regression coefficients and

their ratios. For RB Series 2, the standardized coefficients (0.30*F*, 0.36*R*, -0.54*E<sub>s</sub>*) demonstrate that steric and electronic effects have roughly equal effects on  $pK_a$  values, with  $E_s$  accounting for 45% of the variance in  $pK_a$  and electronic effects split roughly evenly among field (25% *F*) and resonance (30% *R*). As expected due to the bulkier structure of the R6G xanthene core, the standardized coefficients for R6G Series 3 (0.33*F*, 0.30*R*, -0.81*E<sub>s</sub>*) reveal a greater influence of steric effects, with 56% of the variance in  $pK_a$  due to  $E_s$ , 23% to *F*, and 21% to *R*. For both Series 2 and 3 compounds, regression by Eq.2 demonstrates that a high  $pK_a$  is promoted by substituents that are large and electron-withdrawing by induction and resonance.

Many LFER analyses,<sup>[30]</sup> including recent applications of the Fujita-Nishioka model,<sup>[31]</sup> treat polysubstituted aromatics with the assumption that substituent effects are additive. To determine whether this assumption is valid for our compounds and gain further insight into the structure- $pK_a$  correlation, we prepared a limited set of mono-*ortho*-substituted RB derivatives (Series 4, **10-13**). The  $pK_a$  values of Series 4 compounds (Table 1) are tightly clustered and identical within experimental error, with the exception of one slightly higher value (**10**, Cl). A multiple linear regression performed on the combined set of Series 2 and 4  $pK_a$  values using Eq. 2 (Figure S1) failed to predict the nearly identical Series 4 values and was not as successful at predicting Series 2 values as when these were treated separately. This result suggests that substituent effects in the Series 2 di-*ortho* compounds are much stronger than would be expected based on their mono-*ortho* counterparts and the assumption of additive effects. The extreme steric crowding in di-*ortho*-substituted aromatics has previously been shown to cause anomalously high reactivity compared to mono-*ortho* compounds in a kinetic study of Z-arylhrazones of oxadiazoles by Spisani and coworkers.<sup>[31b]</sup> Here, the di-*ortho*-substituted compounds exhibit substituent effects on their  $pK_a$  values that likewise exceed those expected by simple additivity.

To understand the structural basis for the variance in  $pK_a$  values, we attempted to obtain crystal structures of the di-*ortho*-substituted compounds. Of the Series 2 and 3 compounds, we were able to grow high quality crystals only for **9**, the RB di-*o*-iPr derivative. The obtained crystal structure for **9** shows a remarkable deformation of the xanthene ring system, which is generally expected to be planar. As shown in Figure 6, the xanthene system in **9** is deformed into a shape reminiscent of butterfly wings, with the outside rings of the xanthene bent away from the bulky iPr substituents of the aniline-derived substituent. We quantified the xanthene's

deviation from planarity by averaging the C13-O1-C1-C2 and C1-O1-C13-C12 dihedral angles to obtain a value of 154°. The crystal structure for **5** (RB H) was previously reported in the literature<sup>[32]</sup> and exhibits an average xanthene dihedral of 174°, which is much closer to the expected planar structure. This result suggests that deformation of the xanthene ring structure may be required for high  $pK_a$  values such as that observed for **9**.

To test the deformation- $pK_a$  hypothesis, we used Gaussian<sup>[33]</sup> to calculate optimized geometries for Series 2 compounds at the HF/6-311(d,p) level, which was selected because it yielded structures with dihedral angles that matched those obtained from crystal structures for **5** and **9**. The calculated xanthene dihedral angles (Table 2) decrease (i.e., become more deformed) as substituent size increases. These values show good correlation with the  $E_s$  steric parameter ( $r^2 = 0.872$ , Figure S2), supporting the idea the RSL structure becomes more deformed and more highly strained as the di-*ortho* substituents increase in size. We found 6 additional literature crystal structures for RB-based spiro lactams derived from mono-*ortho*-substituted anilines.<sup>[34]</sup> The xanthene dihedral angle was  $>170^\circ$  for all of these compounds except for one with an *o*-SMe substituent<sup>[34c]</sup> that had a slightly more deformed dihedral angle (166°). Thus, it appears that di-*ortho* substitution is required to obtain the most deformed structures (dihedral  $< 160^\circ$ ), which are those with the highest  $pK_a$  values.

The effect of the xanthene deformation and substituent electronics on the  $pK_a$  can be rationalized in conjunction with the mechanism shown in Scheme 1. Protonation of the closed form is expected to be rapid and at equilibrium prior to the ring-opening reaction.<sup>[35]</sup> Thus, differences in closed-open equilibrium are likely driven by the relative thermodynamic stabilities of the protonated intermediate and the fluorescent forms of the dye, which include two tautomers that are indistinguishable by fluorescence. With its delocalized positive charge, the protonated spirocyclic intermediate is destabilized by substituents in the spiro lactam R group that are electron withdrawing by induction or resonance. Stephenson and coworkers previously observed the same electronic effect on the thermodynamic stabilities of a series of pyridine-substituted RSLs, noting that the equilibrium shifted to the open form of the dye as the electron-withdrawing nature of the R group increased.<sup>[36]</sup> The protonated intermediate for our di-*o*-substituted compounds would be additionally destabilized by deformation of its xanthene ring structure as described above. Both the electronic and structural forms of destabilization are expected to be relieved by the spirocyclic ring-opening reaction, which yields a less sterically congested product

in which the positive charge is more extensively delocalized. To probe the effect of substituents that are both electronically and sterically destabilizing, we attempted to synthesize the RB di-*o*-NO<sub>2</sub> derivative, which has a predicted  $pK_a$  value of 8.04 according to Eq. 4A, the regression equation for RB di-*ortho*-substituted compounds. However, our efforts were unsuccessful, perhaps because the spirocyclic form is simply too destabilized for the desired product to form.

Having demonstrated that we can vary the  $pK_a$  of RSLs in systematic fashion via substituent effects, we next set out to assess the general suitability of these RSLs for practical applications. The utility of RSL dyes is often limited by two key features, solubility and single-color emission. Most RSLs have negligible water solubility in their closed forms and frequently require an organic cosolvent. Indeed, **1-19** were titrated in 1:1 v/v EtOH:H<sub>2</sub>O for this reason. RSLs like **1-19** can report on the pH of their surrounding medium as demonstrated above, but this measurement is of fluorescence intensity at a single wavelength. Fluorescence intensity during such measurements can be affected by factors unrelated to the pH, including differences in probe concentration and instrumental or environmental fluctuations. Ratiometric measurements address this problem by using a ratio of fluorescence intensities from two different fluorophores in place of the single-wavelength measurement. Although ratiometric measurements are more desirable for this reason, they exacerbate solubility problems because covalently attaching an additional fluorophore to an RSL further reduces its water solubility in most cases.

An ideal RSL pH probe would be capable of ratiometric sensing in an aqueous environment without organic cosolvent. We developed highly fluorescent conjugated polymer nanoparticles (CPNs) doped with **9** that meet these criteria. CPNs are stably suspended in water, and those that are non-covalently doped with fluorogenic dyes can be employed as ratiometric sensors.<sup>[37]</sup> Undoped CPNs of the conjugated polymer PFBT emit green-yellow fluorescence ( $\lambda_{\max,fl} = 535$  nm) that overlaps the absorbance of RSLs like **9** ( $\lambda_{\max,abs} = 561$  nm), making the CPNs and **9** a suitable fluorescence resonance energy transfer (FRET) donor-acceptor pair. At high pH, all **9** dyes will be in their non-fluorescent spirocyclic form, and only green-yellow fluorescence from the CPNs will be observed (Figure 7A). As the pH is lowered into **9**'s responsive range, **9** dyes will begin to convert to their rhodamine forms, activating FRET from CPN donor chromophores to **9**. As more **9** dyes open, CPN fluorescence will decrease, and orange fluorescence from **9** will increase. In the context of ratiometric pH sensing with RSLs,

the CPNs have two key advantages over most small molecule FRET donors: 1) they are stably suspended in water, obviating the need for an organic cosolvent and 2) they act as light harvesters,<sup>[38]</sup> amplifying the fluorescence intensity of the rhodamine acceptor dyes beyond what would be observed upon direct excitation of the dye. These features have been observed previously in similar CPNs doped with a pH-sensitive fluorescein derivative.<sup>[39]</sup>

Doped CPNs with an average diameter of 14.7 +/- 1.5 nm (Figure S4) were titrated to determine the response of their fluorescence to pH changes. As the pH was lowered, fluorescence intensity from the CPNs decreased while that of **9** increased, and an isoemissive point was observed at 559 nm (Figure 7B). These as-expected changes indicate FRET from the CPNs to **9** as the dyes are converted to their rhodamine form by acid. The fluorescence changes are quantified by the ratio of fluorescence intensity of **9** at 577 nm to that of the CPNs at 535 nm as a function of pH. Figure 7C shows ratiometric data from two representative samples, each of which was titrated from high to low pH with acid and then from low to high pH with base. At pH <4.7, the CPNs exhibit changes in their absorbance spectra consistent with irreversible structural changes, so we focused on the pH 4.7 – 10 range. The relationship between the  $I_{577}/I_{535}$  ratio and pH shows no dependence on the direction of titration, is consistent across the different datasets, and has the appearance of a partial titration curve. Since the ratio continues to increase at the low pH end of the titrations, we could not establish a  $pK_a$  for **9** in the aqueous environment of the nanoparticles. However, the ratio serves as a tool for pH readout within the 4.7 – 10 range, similar to the 5.0 – 8.0<sup>[39b]</sup> and 4.8 – 13<sup>[40]</sup> ranges given for previous CPN-based pH sensors.

An additional feature of the doped CPNs is their ability to amplify the fluorescence intensity of **9**. CPNs have extremely large extinction coefficients and exhibit exciton diffusion that funnels FRET donor energy to acceptor dyes with unusually high efficiency.<sup>[38]</sup> The resulting amplification of acceptor intensity can be quantified by recording the fluorescence of each sample twice, once upon excitation of the dyes via FRET from the CPNs ( $\lambda_{exc} = 450$  nm) and again upon direct excitation of the dyes ( $\lambda_{exc} = 535$  nm). Figure 7D shows that the fluorescence intensity of **9** in a representative sample of doped CPNs is 25 times greater when excited via FRET than when excited directly. This amplification translates to stronger signal and/or the ability to reduce excitation intensity when using CPNs as pH sensors.

## Conclusions

We have demonstrated that the pH responsiveness of aniline-derived RSLs can be systematically tuned via substituent effects. Di-*ortho*-substituted RB- and R6G-derived pH probes exhibit  $pK_a$  values that span the biologically relevant pH 4 – 6 range. LFER analysis using the Fujita-Nishioka model indicates that 45% (RB) to 56% (R6G) of the variance in  $pK_a$  is due to substituent steric effects, with the remainder attributed to inductive and resonance effects. Increasing the size and electron-withdrawing character of the substituents shifts the  $pK_a$  to higher values. Crystal structures and calculated geometries suggest that di-*ortho*-substitution induces deformation of the xanthene moiety to an extent that depends on substituent size. We explored the applicability of RSLs to ratiometric pH sensing in a purely aqueous environment by preparing RSL-doped conjugated polymer nanoparticles. The doped CPNs yielded a consistent ratiometric fluorescence response across the pH 4.7 – 10 range and exhibited a substantial enhancement of rhodamine fluorescence intensity due to the light harvesting effect of the nanoparticles. These results will guide future efforts to develop RSL-based pH probes with  $pK_a$  values targeted to specific processes.

## Experimental Section

**Absorbance and fluorescence studies.** Absorbance and fluorescence measurements were made on a Varian Cary50 and Varian Eclipse, respectively. Stock solutions of **1-19** were prepared in 1:1 (v/v) ethanol:water at a concentration of 20  $\mu\text{M}$  or 2  $\mu\text{M}$  (**4**, **8**, **14-19**) and were stirred at room temperature for 1 h prior to absorbance and fluorescence studies. Absorption and fluorescence titrations were conducted by adding small aliquots of 0.1 M HCl or 0.1 M NaOH to a stirring stock solution (100 mL) of **1-19**. Aliquots were removed for spectroscopic measurement ( $\lambda_{\text{exc,fl}} = 535 \text{ nm}$ ) after the pH stabilized and were then returned to the stock solution. Reported  $pK_a$  values are the average of a minimum of 4 separate titration experiments.

**Materials and methods.** Reagents were purchased from Acros and used as received except 2,6-diethoxyaniline, which was synthesized by a literature procedure.<sup>[41]</sup> Poly[9,9-dioctylfluorenyl-2,7-diyl)-co-1,4-benzo-{2,1'-3}-thiadiazole)] (PFBT) with an average molecular weight of 138,000 and polydispersity 3.1 was obtained from American Dye Source (Quebec, Canada) and used as received. Granular poly(vinyl butyral-co-vinyl alcohol-co-vinyl acetate) (PVB-VA-VA)

was obtained from Sigma-Aldrich.  $^1\text{H}$  and proton-decoupled  $^{13}\text{C}$  NMR spectra were recorded on a Varian Mercury 400 ( $^1\text{H}$  400 MHz,  $^{13}\text{C}$  100 MHz) and referenced to TMS ( $^1\text{H}$ ) or  $\text{CDCl}_3$  at 77.0 ppm ( $^{13}\text{C}$ ). Chemical shifts are reported in ppm and coupling constants in Hz. Mass spectra were measured through positive electrospray ionization (w/ NaCl) on a Bruker 12 Tesla APEX-Qe FTICR-MS with and Apollo II ion source.

**Conjugated polymer nanoparticle preparation and characterization.** Stock solutions of conjugated polymer PFBT (1 mg/mL) and stabilizing polymer PVB-VA-VA (1 mg/mL) in anhydrous THF were stirred overnight under argon. A precursor solution was prepared by combining portions of the PFBT and PVB-VA-VA solutions with additional THF to a final concentration of 0.040 mg/mL PFBT and 0.016 mg/mL PVB-VA-VA. This precursor solution was filtered through a 0.7  $\mu\text{m}$  filter to remove any aggregates and then sonicated for 30 s to ensure homogeneity. A portion of the precursor solution (1 mL) was injected into sonicating ultrapure water (8 mL), and the resulting aqueous suspension of CPNs was sonicated for an additional 2 min. Argon was bubbled through the CPN suspension on a 65  $^\circ\text{C}$  hot plate for 30 min. to remove THF. To dope the CPNs with RSL **9**, a solution of **9** in THF (3.6  $\mu\text{L}$ , 10 mg/mL) was injected into the CPN suspension. The aqueous suspension of **9**-doped CPNs was then filtered through a 0.22  $\mu\text{m}$  filter to remove any aggregated dyes or CPNs. CPN size distributions were measured in aqueous suspension by dynamic light scattering using a Nicomp N3000 Submicron Particle Sizer (Particle Sizing Systems), and the size distribution is shown in Figure S4. Titrations of **9**-doped CPNs were conducted by adding small aliquots of 2.5 mM HCl or 5 mM NaOH to a 2.5 mL portion of the aqueous dispersion of CPNs in a quartz cuvette. After the pH stabilized, absorption and fluorescence spectra were recorded. Ratios of peak fluorescence intensities were computed using IgorPro 6.05.

**General synthetic procedures.** Compounds **1**, **2**, and **5** were reported previously.<sup>[17]</sup> Detailed characterization data for compounds **3-4** and **6-19** are given in the Supporting Information. To prepare compounds **3-4** and **6-13**, phosphorus oxychloride (3 mmol) was added dropwise to a stirred solution of rhodamine B (0.6 mmol) in 1,2-dichloroethane (8 mL). The desired aniline (1 mmol) was added dropwise, and the reaction mixture was refluxed for 24 hours. The solution was washed with 2 M HCl (2x), 2 M NaOH (3x), and brine (2x). The organic layer was dried

with MgSO<sub>4</sub> and concentrated *in vacuo*. The crude product was purified by manual flash column chromatography.

To prepare compounds **14-19**, the carboxylic acid form of rhodamine 6G (0.5 mmol) was dissolved in anhydrous 1,2-dichloroethane (60 mL) with sonication and added to a flame-dried round bottom flask equipped with molecular sieves. After stirring overnight under argon, the solution was placed in an ice bath, and the desired aniline (3 mmol) was added and stirred for 30 min. Phosphorous oxychloride (0.5 mmol) was added dropwise, and the mixture was stirred for 48 hours. The solution was filtered and then washed with chilled 2M NaOH (3x) and brine (1x). After drying with Na<sub>2</sub>SO<sub>4</sub>, the solution was concentrated *in vacuo*. The crude product was purified by manual flash column chromatography.

## Acknowledgements

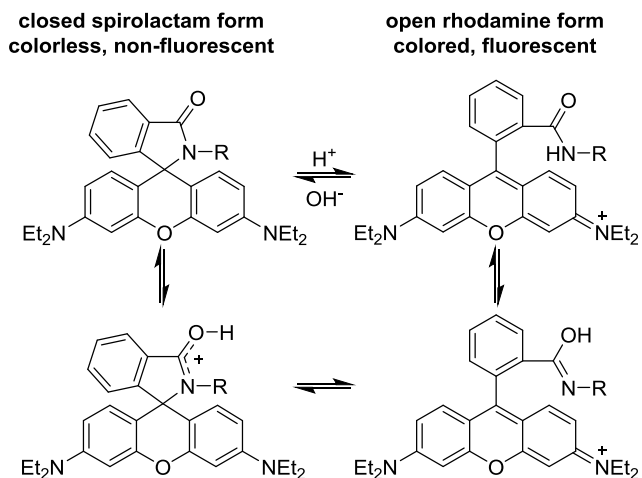
We gratefully acknowledge support of this work by the Camille and Henry Dreyfus Foundation through a Henry Dreyfus Teacher-Scholar Award; the National Science Foundation (CHE-1464699); and the Charles Center of the College of William and Mary *via* student fellowships (G.H.T., S.G.S, M.R.). We thank Prof. Robert D. Pike of the College of William and Mary for the x-ray crystal structure.

## References

- [1] F. B. Loiseau, J. R. Casey, *Methods Mol. Biol.* **2010**, *637*, 311-331.
- [2] J. Han, K. Burgess, *Chem. Rev.* **2010**, *110*, 2709-2728.
- [3] J. R. Casey, S. Grinstein, J. Orłowski, *Nat Rev Mol Cell Biol* **2010**, *11*, 50-61.
- [4] B. A. Webb, M. Chimenti, M. P. Jacobson, D. L. Barber, *Nat Rev Cancer* **2011**, *11*, 671-677.
- [5] a) J. Yin, Y. Hu, J. Yoon, *Chem Soc Rev* **2015**, *44*, 4619-4644; b) Y. Ni, J. Wu, *Org Biomol Chem* **2014**, *12*, 3774-3791; c) N. Boens, V. Leen, W. Dehaen, *Chem Soc Rev* **2012**, *41*, 1130-1172; d) R. Wang, C. Yu, F. Yu, L. Chen, C. Yu, *TrAC, Trends Anal. Chem.* **2010**, *29*, 1004-1013.
- [6] X. Chen, T. Pradhan, F. Wang, J. S. Kim, J. Yoon, *Chem. Rev.* **2012**, *112*, 1910-1956.
- [7] M. Beija, C. A. M. Afonso, J. M. G. Martinho, *Chem. Soc. Rev.* **2009**, *38*, 2410-2433.
- [8] Z. Yang, J. Cao, Y. He, J. H. Yang, T. Kim, X. Peng, J. S. Kim, *Chem. Soc. Rev.* **2014**, *43*, 4563-4601.
- [9] a) H.-S. Lv, S.-Y. Huang, Y. Xu, X. Dai, J.-Y. Miao, B.-X. Zhao, *Bioorg. Med. Chem. Lett.* **2014**, *24*, 535-538; b) H. Li, C. Wang, M. She, Y. Zhu, J. Zhang, Z. Yang, P. Liu, Y. Wang, J. Li, *Anal. Chim. Acta* **2015**, *900*, 97-102; c) X.-L. Shi, G.-J. Mao, X.-B. Zhang, H.-W. Liu, Y.-J. Gong, Y.-X. Wu, L.-Y. Zhou, J. Zhang, W. Tan, *Talanta* **2014**,

- 130, 356-362; d) K.-K. Yu, K. Li, J.-T. Hou, H.-H. Qin, Y.-M. Xie, C.-H. Qian, X.-Q. Yu, *RSC Adv.* **2014**, *4*, 33975-33980; e) H. Li, H. Guan, X. Duan, J. Hu, G. Wang, Q. Wang, *Org. Biomol. Chem.* **2013**, *11*, 1805-1809.
- [10] a) J.-L. Tan, F. Zhang, T.-T. Yang, Y. Liu, M.-X. Zhang, Z.-B. Li, H. Zuo, *Spectrochim Acta A Mol Biomol Spectrosc* **2015**, *140*, 489-494; b) Z.-Q. Hu, M. Li, M.-D. Liu, W.-M. Zhuang, G.-K. Li, *Dyes Pigm.* **2013**, *96*, 71-75; c) M. Devi, A. Dhir, C. P. Pradeep, *Eur. J. Org. Chem.* **2015**, *2015*, 4650-4657; d) A. Liu, M. Hong, W. Yang, S. Lu, D. Xu, *Tetrahedron* **2014**, *70*, 6974-6979; e) M.-C. Xia, L. Cai, S. Zhang, X. Zhang, *Anal. Chem.* **2017**, *89*, 1238-1243; f) H. Yu, G. Li, B. Zhang, X. Zhang, Y. Xiao, J. Wang, Y. Song, *Dyes Pigm.* **2016**, *133*, 93-99; g) Y. Xue, W. Liang, Y. Li, Y. Wu, X. Peng, X. Qiu, J. Liu, R. Sun, *J. Agric. Food. Chem.* **2016**, *64*, 9592-9600.
- [11] M. H. Lee, J. H. Han, J. H. Lee, N. Park, R. Kumar, C. Kang, J. S. Kim, *Angew. Chem., Int. Ed.* **2013**, *52*, 6206-6209.
- [12] a) X.-F. Zhang, T. Zhang, S.-L. Shen, J.-Y. Miao, B.-X. Zhao, *RSC Advances* **2015**, *5*, 49115-49121; b) U. Reddy G, A. H. A, F. Ali, N. Taye, S. Chattopadhyay, A. Das, *Org. Lett.* **2015**, *17*, 5532-5535; c) N. I. Georgiev, A. M. Asiri, A. H. Qusti, K. A. Alamry, V. B. Bojinov, *Dyes Pigm.* **2014**, *102*, 35-45; d) J. Fan, C. Lin, H. Li, P. Zhan, J. Wang, S. Cui, M. Hu, G. Cheng, X. Peng, *Dyes Pigm.* **2013**, *99*, 620-626; e) S.-L. Shen, X.-F. Zhang, S.-Y. Bai, J.-Y. Miao, B.-X. Zhao, *RSC Adv.* **2015**, *5*, 13341-13346.
- [13] J. Hu, L. Dai, S. Liu, *Macromolecules* **2011**, *44*, 4699-4710.
- [14] C. Rivas, G. J. Stasiuk, J. Gallo, F. Minuzzi, G. A. Rutter, N. J. Long, *Inorg. Chem.* **2013**, *52*, 14284-14293.
- [15] X. Zhao, X. Jia, L. Liu, J. Zeng, K. Tian, T. Zhou, P. Liu, *Biomacromolecules* **2016**, *17*, 1496-1505.
- [16] L. Yuan, W. Lin, Y. Feng, *Org. Biomol. Chem.* **2011**, *9*, 1723-1726.
- [17] W. L. Czaplinski, G. E. Purnell, C. A. Roberts, R. M. Allred, E. J. Harbron, *Org. Biomol. Chem.* **2014**, *12*, 526-533.
- [18] a) Q. A. Best, C. Liu, P. D. van Hoveln, M. E. McCarroll, C. N. Scott, *J. Org. Chem.* **2013**, *78*, 10134-10143; b) A. Bender, Z. R. Woydziak, L. Fu, M. Branden, Z. Zhou, B. D. Ackley, B. R. Peterson, *ACS Chem. Biol.* **2013**, *8*, 636-642.
- [19] C. Liu, Q. A. Best, B. Suarez, J. Pertile, M. E. McCarroll, C. N. Scott, *J. Fluoresc.* **2015**, *25*, 231-237.
- [20] E. S. Childress, C. A. Roberts, D. Y. Sherwood, C. L. M. LeGuyader, E. J. Harbron, *Anal. Chem.* **2012**, *84*, 1235-1239.
- [21] R. F. Kubin, A. N. Fletcher, *J. Lumin.* **1982**, *27*, 455-462.
- [22] S. Winstein, N. J. Holness, *J. Am. Chem. Soc.* **1955**, *77*, 5562-5578.
- [23] R. W. Taft, Jr., in *Steric effects in organic chemistry* (Ed.: M. S. Newman), John Wiley & Sons, New York, **1956**, pp. 556-675.
- [24] E. Kutter, C. Hansch, *J. Med. Chem.* **1969**, *12*, 647-652.
- [25] M. Charton, *Prog. Phys. Org. Chem* **1971**, *8*, 235-318.
- [26] T. Fujita, T. Nishioka, *Prog. Phys. Org. Chem* **1976**, *12*, 49-89.
- [27] C. G. Swain, E. C. Lupton, *J. Am. Chem. Soc.* **1968**, *90*, 4328-4337.
- [28] C. Hansch, A. Leo, S. H. Unger, K. H. Kim, D. Nikaitani, E. J. Lien, *J. Med. Chem.* **1973**, *16*, 1207-1216.

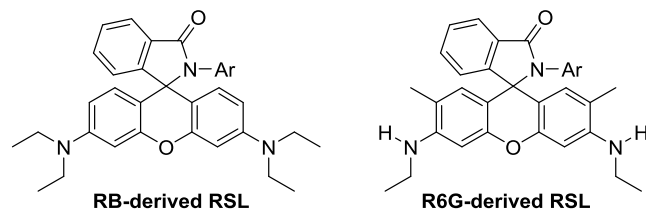
- [29] Additional regressions were run with recalculated F and R values from C. Hansch, A. Leo and R.W. Taft, *Chem. Rev.*, **1991**, *91*, 165, but these values did not appreciably alter the regression equation or significance.
- [30] H. H. Jaffé, *Chem. Rev.* **1953**, *53*, 191-261.
- [31] a) R. Grainger, J. Cornella, D. C. Blakemore, I. Larrosa, J. M. Campanera, *Chemistry – A European Journal* **2014**, *20*, 16680-16687; b) F. D'Anna, F. Ferroni, V. Frenna, S. Guernelli, C. Z. Lanza, G. Macaluso, V. Pace, G. Petrillo, D. Spinelli, R. Spisani, *Tetrahedron* **2005**, *61*, 167-178; c) F. D'Anna, V. Frenna, C. Z. Lanza, G. Macaluso, S. Marullo, D. Spinelli, R. Spisani, G. Petrillo, *Tetrahedron* **2010**, *66*, 5442-5450.
- [32] W.-J. Deng, D. Sun, B.-Y. Su, S.-P. Wang, H. Zheng, *Acta Crystallogr. Sect. E: Struct. Rep. Online* **2009**, *65*, o1464-o1464.
- [33] Gaussian 09, Revision D.01, M. J. Frisch, G. W. Trucks, H. B. Schlegel, G. E. Scuseria, M. A. Robb, J. R. Cheeseman, G. Scalmani, V. Barone, G. A. P. B. Mennucci, H. Nakatsuji, M. Caricato, X. Li, H. P. Hratchian, A. F. Izmaylov, J. Bloino, G. Zheng, J. L. Sonnenberg, M. Hada, M. Ehara, K. Toyota, R. Fukuda, J. Hasegawa, M. Ishida, T. Nakajima, Y. Honda, O. Kitao, H. Nakai, T. Vreven, J. A. Montgomery, Jr., J. E. Peralta, F. Ogliaro, M. Bearpark, J. J. Heyd, E. Brothers, K. N. Kudin, V. N. Staroverov, R. Kobayashi, J. Normand, K. Raghavachari, A. Rendell, J. C. Burant, S. S. Iyengar, J. Tomasi, M. Cossi, N. Rega, J. M. Millam, M. Klene, J. E. Knox, J. B. Cross, V. Bakken, C. Adamo, J. Jaramillo, R. Gomperts, R. E. Stratmann, O. Yazyev, A. J. Austin, R. Cammi, C. Pomelli, J. W. Ochterski, R. L. Martin, K. Morokuma, V. G. Zakrzewski, G. A. Voth, P. Salvador, J. J. Dannenberg, S. Dapprich, A. D. Daniels, O. Farkas, J. B. Foresman, J. V. Ortiz, J. Cioslowski, and D. J. Fox, Gaussian, Inc., Wallingford CT, **2009**.
- [34] a) P. Du, S. J. Lippard, *Inorg. Chem.* **2010**, *49*, 10753-10755; b) H. Zheng, G.-Q. Shang, S.-Y. Yang, X. Gao, J.-G. Xu, *Org. Lett.* **2008**, *10*, 2357-2360; c) M. Yang, W. Meng, Q. Ding, N. Su, X. Liu, M. Zhang, B. Yang, *New J. Chem.* **2015**, *39*, 4790-4795; d) N. Chatterjee, S. B. Maity, A. Samadder, P. Mukherjee, A. R. Khuda-Bukhsh, P. K. Bharadwaj, *RSC Advances* **2016**, *6*, 17995-18001; e) Y. Long, in *CSD Communication*, **2016**.
- [35] H. Montenegro, M. Di Paolo, D. Capdevila, P. F. Aramendia, M. L. Bossi, *Photochem. Photobiol. Sci.* **2012**, *11*, 1081-1086.
- [36] M. J. Maher, K. Yehl, F. Haque, A. Faint, K. D. Shimizu, C. J. Stephenson, *Sens. Actuators, B* **2014**, *200*, 1-8.
- [37] Z. Tian, J. Yu, C. Wu, C. Szymanski, J. McNeill, *Nanoscale* **2010**, *2*, 1999-2011.
- [38] Y. Jiang, J. McNeill, *Chem. Rev.* **2017**, *117*, 838-859.
- [39] a) W. Xu, S. Lu, M. Xu, Y. Jiang, Y. Wang, X. Chen, *J. Mater. Chem. B* **2016**, *4*, 292-298; b) Y.-H. Chan, C. Wu, F. Ye, Y. Jin, P. B. Smith, D. T. Chiu, *Anal. Chem.* **2011**, *83*, 1448-1455.
- [40] H. Cui, Y. Chen, L. Li, Y. Wu, Z. Tang, H. Fu, Z. Tian, *Microchimica Acta* **2014**, *181*, 1529-1539.
- [41] W. R. Carroll, C. Zhao, M. D. Smith, P. J. Pellechia, K. D. Shimizu, *Org. Lett.* **2011**, *13*, 4320-4323.



**Scheme 1.** RSL acid-base equilibrium.

**Table 1.** RSL derivatives and  $pK_a$  values.

Aniline	RB cmpd #	RB $pK_a$	R6G cmpd #	R6G $pK_a$
4-Cl	1	4.21 ± 0.01		
2,6-Cl <sub>2</sub> -4-NO <sub>2</sub>	2	5.46 ± 0.03		
3,5-Cl <sub>2</sub>	3	4.34 ± 0.05		
2,6-Cl <sub>2</sub>	4	5.38 ± 0.08	14	5.62 ± 0.04
H	5	4.31 ± 0.02	15	3.81 ± 0.02
2,6-F <sub>2</sub>	6	4.52 ± 0.08	16	4.30 ± 0.04
2,6-OEt <sub>2</sub>	7	4.03 ± 0.07	17	4.15 ± 0.05
2,6-Me <sub>2</sub>	8	4.90 ± 0.11	18	5.32 ± 0.07
2,6-iPr <sub>2</sub>	9	5.72 ± 0.13	19	5.87 ± 0.06
2-Cl	10	4.43 ± 0.08		
2-F	11	4.33 ± 0.01		
2-Me	12	4.31 ± 0.02		
2-iPr	13	4.28 ± 0.02		



Scheme 2. RSL structures.

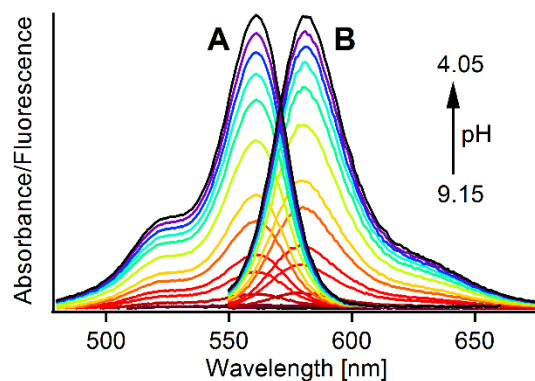


Figure 1. Absorption (A) and fluorescence (B) of compound **9** in 1:1 (v/v) ethanol-water during titration between pH 9.15 and 4.05.

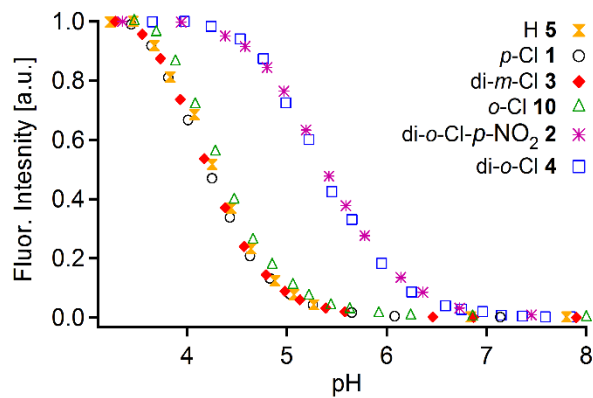
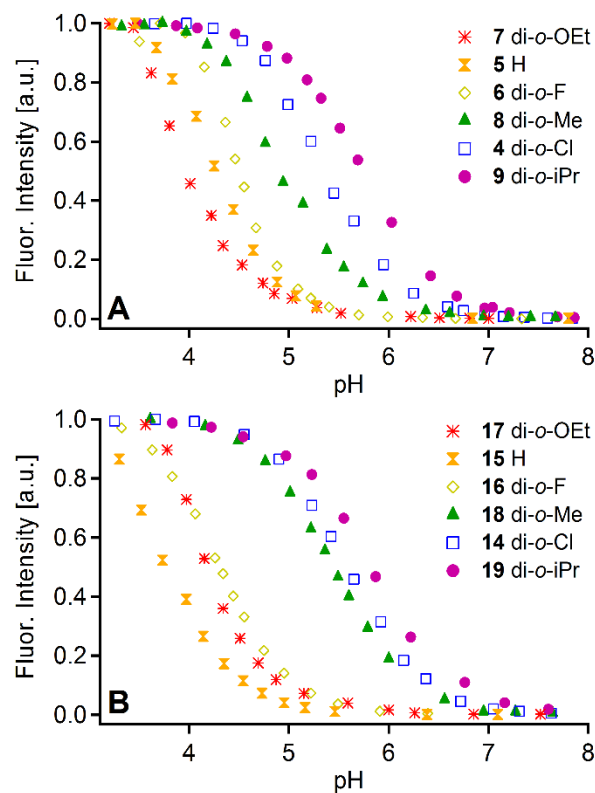
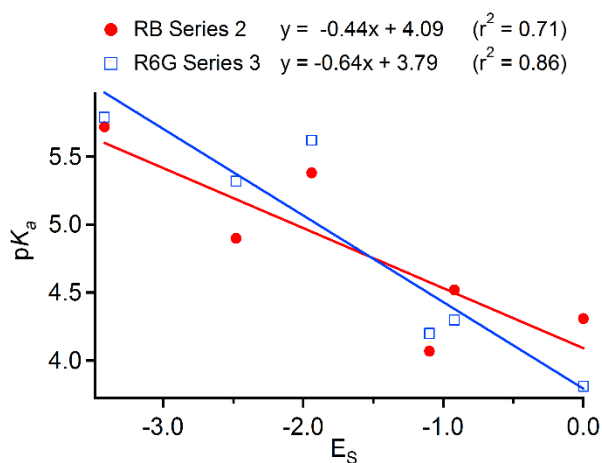


Figure 2. Normalized fluorescence intensity at the  $\lambda_{\max,fl}$  as a function of pH for Series 1 compounds in 1:1 v/v ethanol-water.



**Figure 3.** Normalized fluorescence intensity at the  $\lambda_{\max,fl}$  as a function of pH for RB Series 2 (A) and R6G Series 3 (B) compounds in 1:1 v/v ethanol-water.



**Figure 4.** Experimental  $pK_a$  values for RB Series 2 (red) and R6G Series 3 (blue) compounds vs. the Taft-Kutter-Hansch  $E_s$  steric parameter.

Table 2. Substituent parameters for LFER analysis.					
Substituent	$E_s^{[a]}$	$\sigma_p^{[a]}$	$F^{[a]}$	$R^{[a]}$	angle <sup>[b]</sup>
Cl	-0.97	0.23	0.41	-0.15	155 (4)
H	0	0	0	0	173 (5)
F	-0.46	0.06	0.43	-0.34	169 (6)
OEt	-0.55	-0.24	0.22	-0.44	162 (7)
Me	-1.24	-0.17	-0.04	-0.13	155 (8)
iPr	-1.71	-0.15	-0.05	-0.10	152 (9)

[a] Parameters derived from ref. 26. Parameters were doubled in analyses of di-*ortho*-substituted compounds.

[b] Calculated xanthene angles for the designated derivatives as described in the text.

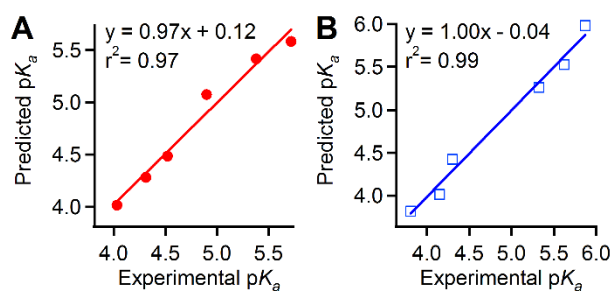


**Figure 5.** Predicted vs. experimental  $pK_a$  values for RB Series 2 (A) and R6G Series 3 (B) compounds. Predicted values were obtained by multiple linear regression according to the modified Fujita-Nishioka model in Eq. 2.

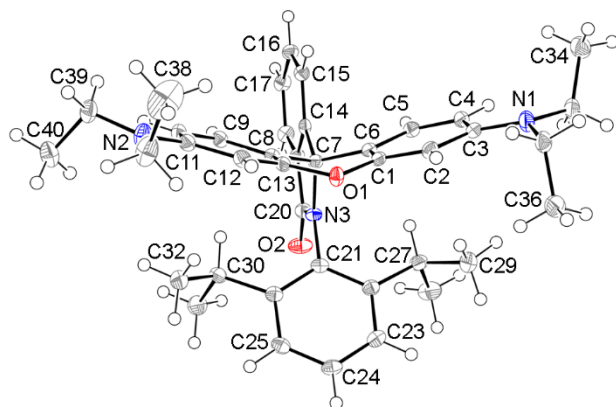


**Figure 6.** Crystal structure of **9**.

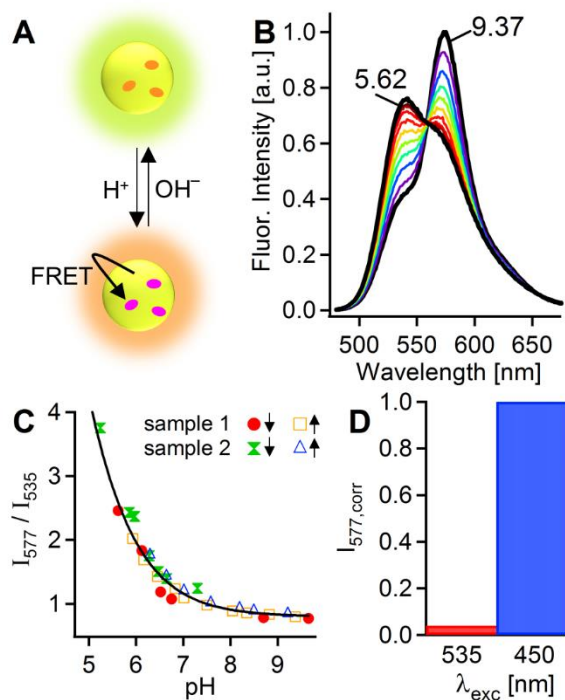


**Figure 7.** (A) Graphic representation of **9**-doped CPNs with pH-dependent ratiometric fluorescence properties. (B) Fluorescence spectra of **9**-doped CPNs in aqueous suspension as a function of pH, where the spectra with the highest and lowest pH values are shown in black and labeled with their pH values. (C) Ratio of **9** to CPN fluorescence intensities ( $I_{577}/I_{535}$ ) as a function of pH for 2 separate samples during titrations from high to low pH with acid (red and green symbols) and from low to high pH with base (orange and blue symbols). The sigmoidal curve is presented as a guide to the eye. (D) Relative fluorescence intensity of **9** at 577 nm at pH 5.11 when excited directly at 535 nm (red) or via FRET from the CPNs at 450 nm (blue). The fluorescence intensities were corrected for CPN emission at 577 nm.